WAVE-DRIVEN VORTEX PATTERNS AT AN OPEN BEACH

Andreas Bondehagen[1], Volker Roeber[2 3], Henrik Kalisch [1], Marc P. Buckley [4], Michael Streßer [4], Marius Cysewski [4], Jochen Horstmann [4], Maria Bjørnestad [5], Olufemi E. Ige [1], Hege G. Frøysa [6], Ruben Carrasco-Alvarez [4]

This contribution is structured in two parts: a concise summary of the key findings from the original study (Bondehagen et al. (2024)) and an exploration of some open-ended questions concerning tracer paths in the surfzone. The Boussinesq-type model BOSZ is validated against field measurements, demonstrating its effectiveness in capturing wave-driven surf zone dynamics. The influence of tidal elevation, wave direction, and directional spread on vortex size and strength is examined, highlighting the interplay between wave propagation and bathymetry. Building on these findings, the remainder of this paper delves deeper into vortex behavior using Lagrangian tracers and presents preliminary insights into chaotic motion in the surf zone, further advancing our understanding of nearshore wave dynamics.

Keywords: Surf zone circulation; Boussinesq-type model; Rankine Vortex; Surface tracers

INTRODUCTION

The nearshore environment is characterized by complex hydrodynamic processes resulting from the interaction of waves, currents, and coastal topography. In this highly dynamic zone, wave-driven currents play a central role in shaping circulation patterns, including flows along the shore and over the shore, rip currents, and vortex formation of multiple spatial and temporal scales (Putrevu and Svendsen, 1999; Svendsen, 2006; Castelle et al., 2016). Understanding these circulation patterns is crucial as they strongly influence sediment transport, coastal morphology, and beach erosion (Inman and Brush, 1973; Davidson-Arnott et al., 2019; Roberts et al., 2014; Nader et al., 2017), as well as the distribution of nutrients, microorganisms, and pollutants in the nearshore zone (Rilov et al., 2008; Shanks et al., 2010; Brown et al., 2015; Larsen et al., 2023). In addition, nearshore currents, and especially rip currents, have significant implications for beach safety, often creating hazardous conditions for swimmers and prompting the need for improved coastal hazard management (Castelle et al., 2016).

In recent decades, numerical modeling has emerged as an essential tool for studying surf zone hydrodynamics and nearshore circulation. In particular, phase-resolving Boussinesq-type and non-hydrostatic models have demonstrated the ability to capture complex wave dynamics, wave breaking, and resulting currents with high fidelity (Chen et al., 2003; Feddersen et al., 2011; Clark et al., 2011; Hally-Rosendahl and Feddersen, 2016; Lynett et al., 2017; Baker et al., 2021). The Boussinesq Ocean and Surf Zone (BOSZ) model introduced in Roeber et al. (2010) and Roeber and Cheung (2012a) is one such model that has been extensively benchmarked and used for a range of nearshore applications, and is adept at computing wave-induced circulation patterns and enabling in-depth analysis of vortex dynamics in the surf zone (Roeber and Cheung, 2012b; Li et al., 2014; Roeber and Bricker, 2015; Filipot et al., 2019; Wong et al., 2019; Morichon et al., 2021; Pinault et al., 2020; Varing et al., 2020; David et al., 2021; Varing et al., 2021; Watanabe et al., 2021; Kalisch et al., 2024).

Vortexes, or horizontal eddies, have garnered considerable interest due to their role in mixing, transport, and exchange processes within the surf zone. Previous observational and modeling studies have shown that Boussinesq-type models can capture the generation and evolution of vortexes associated with wave breaking and the interaction of waves with bathymetric features (Feddersen, 2014; Hally-Rosendahl et al., 2015; Spydell and Feddersen, 2009; Spydell et al., 2009; Suanda and Feddersen, 2015; Choi et al., 2015; O'Dea et al., 2021). For instance, numerical investigations have demonstrated that variations in incoming wave direction, directional spread, and water depth can significantly influence vortex size, strength, and prevalence, as well as the development of transient rip currents and alongshore variability in circulation (Feddersen et al., 2011; Choi et al., 2015; Suanda and Feddersen, 2015; Hally-Rosendahl and Feddersen, 2016; O'Dea et al., 2021). Studies like those by Spydell et al. (2007) and Scott et al. (2014) have also shown that drifters deployed in the surf zone often exhibit complex trajectories that reflect the presence and

[1] Department of Mathematics, University of Bergen, Norway
[2] Université de Pau et des Pays de l'Adour, France
[3] Department of Oceanography, University of Hawaii at Manoa, The United States
[4] Helmholtz-Zentrum Hereon, Germany
[5] The Norwegian Meteorological Institute, Norway
[6] Aqua Kompetanse AS, Norway

evolution of vortical flows, underscoring the connection between vortexes, particle transport, and potential chaotic motion.

In the recent article by Bondehagen et al. (2024), the BOSZ model was validated against a unique set of field measurements at an open beach on Sylt Island, Germany (Bjørnestad et al., 2021). Observations included the use of orange drifters tracked by a stereo-camera system, pressure gauges, and an ADV complemented by wave buoy data offshore. The model successfully replicated nearshore velocity fields and drifter trajectories, thereby confirming its reliability for studying surf zone circulation. Building on this validation, Bondehagen et al. (2024) analyzed how tidal elevation (*tide*), wave directional spread (σ_θ), and peak wave direction (D_P) influence vortex patterns. This study showed that *tide* and D_P affect the number of vortexes, *tide* and σ_θ influence their size, and σ_θ and D_P influence their strength.

Examining how vortex patterns vary with these parameters reveals the mechanisms behind their formation, offering key insights into nearshore circulation, sediment transport, and the coastal retention or dispersion of nutrients and pollutants.

In the present contribution, we first summarize the key findings of Bondehagen et al. (2024), offering a condensed overview of how BOSZ captured the essential features of wave-driven nearshore circulation and vortex dynamics. We then supplement this by showcasing fluid particle movement in the presence of a vortex. In addition, we showcase and discuss the seemingly chaotic movement of fluid particles in the surf zone. For more comprehensive details on the validation methods, numerical procedures, and broader context, the reader is encouraged to consult the full article by Bondehagen et al. (2024) and the supplementary material.

VALIDATION OF BOSZ

A comprehensive field measurement campaign was conducted at a beach on Sylt Island, Germany, in September 2019, to validate the BOSZ model and to study wave-driven currents. This campaign combined data collection from oranges used as drifters, stereo imaging, pressure sensors, an acoustic Doppler velocimeter (ADV), and offshore wave buoy measurements. The integration of these methods allowed for detailed analysis of nearshore circulation patterns under realistic environmental conditions.

Field measurements

The experimental setup used by Bjørnestad et al. (2021) included a series of wave poles deployed along a cross-shore transect at the site, fitted with pressure sensors and an ADV (see Figure 1 for an overview). The ADV was installed to measure near-bed velocities, while the pressure sensors were used to reconstruct surface elevations via the weakly dispersive, non-linear method described by Bonneton et al. (2018).

To measure surface velocities, oranges used as drifters were deployed in the surf zone and tracked using a custom-built stereo imaging system. The cameras, positioned on elevated dunes, recorded drifter movements at 30 frames per second. The stereo imaging system was calibrated using a checkerboard method, before being used for reconstructing 3D world coordinates from the pixel data (Bondehagen et al., 2024). The drifters provided Lagrangian measurements of surf zone currents.

Wave conditions were monitored via the Bunker Hill wave buoy, located offshore at a depth of approximately 10 m. The buoy recorded significant wave height (H_s), peak period (T_p) and directional spreading (σ_θ). On the calmer day (September 8, 2019), (H_s) was 0.74m with a peak period of 9.1 s, providing ideal conditions for tracking drifter trajectories without interference from excessive wave breaking or foam. These conditions were contrasted with data from September 7, 2019, when higher wave energy (H_s = 0.91m) created challenges for drifter tracking due to foam obscuring the drifters in breaking waves.

Buoy and ADV comparison

To validate the BOSZ model, comparisons were made between the computed wave fields and the observational data collected during the field campaign. This included surface elevation and velocity data from the Bunker Hill wave buoy and ADV measurements near Pole 2. The comparisons were divided between the two experimental days, as the conditions for each day made for unique challenges.

On September 7, 2019, wave conditions were characterized by higher energy, with a significant wave height (H_s = 0.91m) and shorter peak period (T_p = 6.5s). These conditions created a surf zone with strong wave breaking and foam, which limited the ability to track the drifters. However, a high tide provided an opportunity to evaluate BOSZ against measured spectra from a buoy and ADV located at the bottom of one of the poles. The model captured the main features of the wave elevation spectra recorded by the

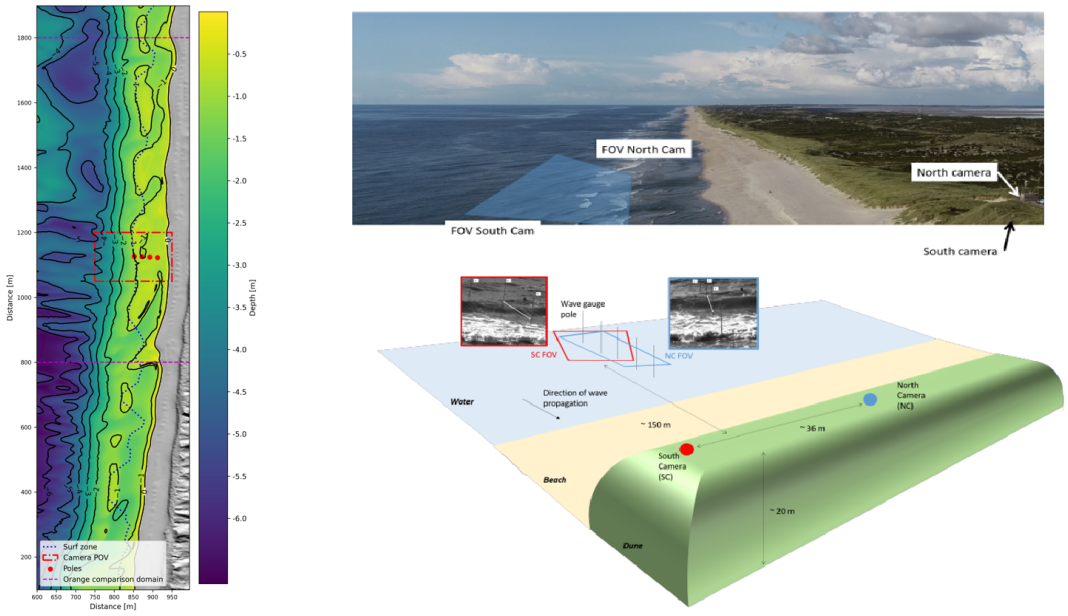

Figure 1: Overview of the experimental and modeling set-up at Sylt. On the right the experimental set-up is shown, showcasing the location and FOV of the stereo cameras, pressure gauges and ADV. To the left the 2 by 1 kilometer modeling bathymetry is shown. The depth is colored, with some contours shown. Additionally, the approximate camera FOV and pole locations are shown. as well as the approximate location of the surf zone found by looking at where numerical wave breaking occurred. For the comparison of orange paths, a smaller domain was chosen to speed up computations.

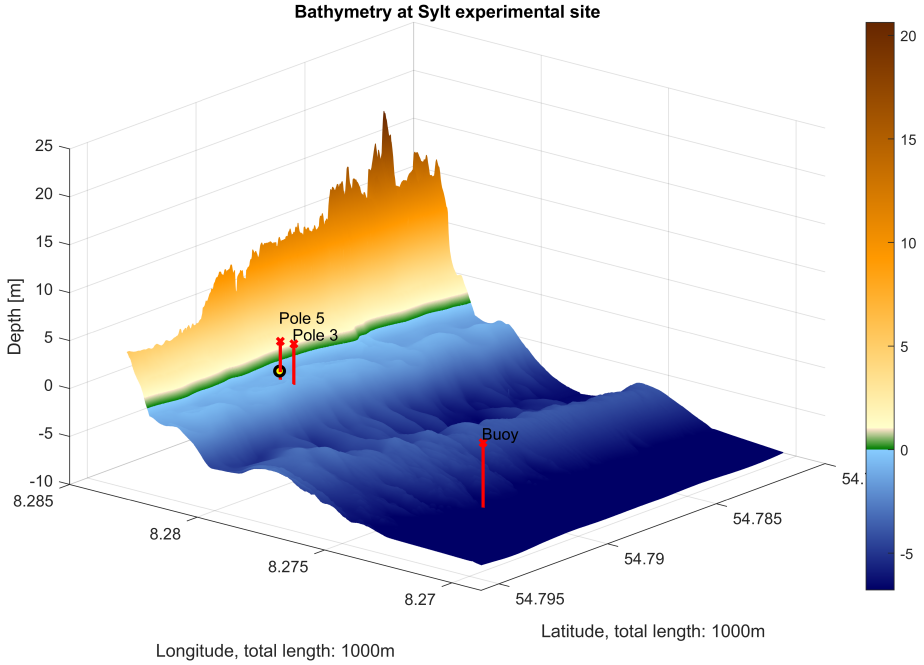

Figure 2: Bathymetry used in the computations for the orange comparison. This bathymetry corresponds to the area between the two purple dashed lines in Figure 1.

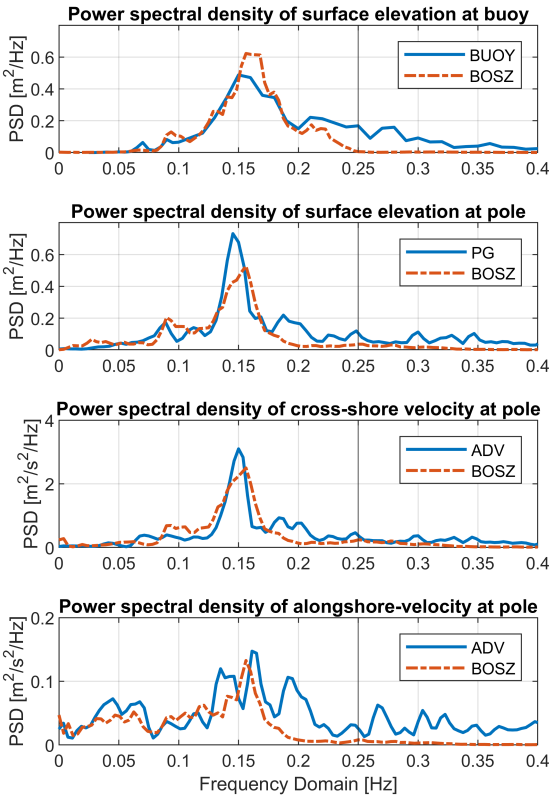

(a) PSD of surface elevation at the buoy, and PSD of surface elevation and velocities at the poles September 7.

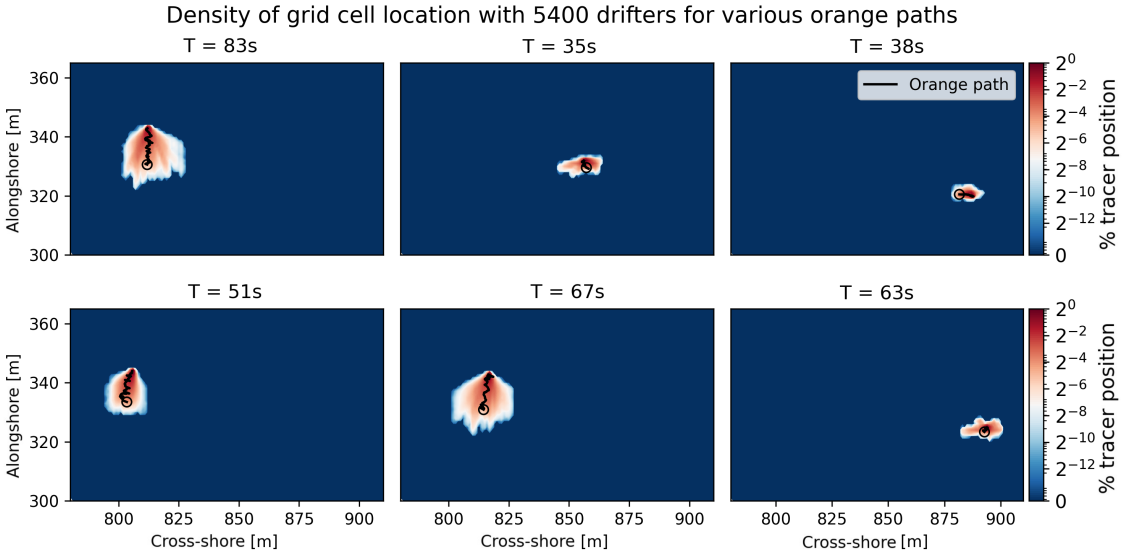

(b) Comparison of numerical particle paths with those of the oranges released on September 8. In black is the reconstructed orange path, and white is the mean of the paths of the numerical intertial particles. The colours represent how many numerical particles went through that location. As can be seen, the numerical particles diverges showcasing chaotic behaviour.

Figure 3: Validation of the BOSZ model. Figure (a) and (b) show the comparison of the PSD of the recorded wave elevation and fluid velocities. The vertical dotted line denote the maximum resolved frequency due to the grid resolution of 2 by 2 meter. Figure (c) shows the comparison of the orange paths compared to the numerical intertial particles. The mean of the numerical paths (white) matches well with the actual path (black).

buoy, although high-frequency energy ($> 0.25Hz$) was redistributed to lower frequencies due to the grid resolution constraints of 2 m by 2 m. Nearshore, comparisons with the pressure sensor and ADV revealed that the model accurately reproduced the shape and peak frequencies of the spectra for surface elevation and cross-shore velocities. However, the alongshore velocity spectra lacked some finer details, likely due to differences in bathymetry and the simplified representation of bottom friction in the model (see Figure 3a).

On September 8, 2019, wave conditions were calmer, with a significant wave height of $H_s = 0.74$m and a peak period of $T_p = 9.1$s. These conditions provided an ideal setting for drifter experiments, as the calmer conditions made for less foam which made tracking the oranges easier with the stereo camera. This comparison can be found in the next section. For this day, only the buoy measurements were available since the low tide meant that the ADV and pressure gauge were outside the water. The buoy's surface elevation spectra showed a peak at the primary wave frequency, which the BOSZ model successfully reproduced (Bondehagen et al., 2024). Although ADV data was not available on this day due to the low tide causing them to be above the sea surface, the agreement between modeled and measured spectra on the first day reinforced confidence in the model's ability to replicate wave dynamics. Overall, these comparisons demonstrated that BOSZ could accurately simulate the energy distribution across wave frequencies and provide reliable inputs for studying nearshore circulation.

Particle path comparison

The orange drifters served as Lagrangian tracers, offering valuable insights into nearshore circulation patterns. The BOSZ model was validated with the observed drifter trajectories through recreation of their paths as numerical inertial particles under the computed wave conditions. As opposed to fluid partices such as studied for example by Borluk and Kalisch (2012), inertial particles are assumed to have finite mass. In this case a different particle drift model must be used (Bakhoday-Paskyabi, 2015). On September 8, 2019, the drifters were deployed in the surf zone and their positions were tracked using the stereo imaging system. The recorded paths were transformed into three-dimensional world coordinates using a calibrated checkerboard method, ensuring precise alignment with the computational domain (see also Bjørnestad et al. (2021)).

To compare the drifter paths, inertial particles were released in the BOSZ model at locations matching the initial deployment points of the drifters after a spin-up time of $T = 500$s. The model used the wave spectra and bathymetry inputs from the field campaign. By averaging over multiple model runs to account for wave phase variability and uncertainties in tide and directional spreading, the BOSZ particles successfully replicated the general patterns observed in the field. The modeled trajectories captured key features of drifter motion, including cross-shore excursions and longshore drift, and aligned well with the measured end positions of the drifters (see Figure 3b).

Despite some deviations in individual paths, the ensemble behavior of the modeled particles closely matches the observed movement. The analysis also revealed that drifters moving outside the sandbar exhibited higher velocities and greater cross-shore variability, while those within the sandbar were more constrained, which is consistent with the wave-driven circulation patterns. This agreement between observed and computed drifter paths highlights BOSZ's capability to accurately account for complex Lagrangian transport in the surf zone.

VORTEX PATTERNS

Methodology

To analyze surf zone vortex dynamics, we employed the BOSZ model to simulate wave-driven circulation under varying wave and tide conditions. The model domain was initialized with high-resolution bathymetry and directional wave spectra obtained during the field campaign. Simulations were run for 3600 seconds, with the first 600 seconds used as a spin-up period to allow for the wave field to reach a steady state. The velocity fields were then averaged over the remaining computed time to identify circulation patterns and detect vortex structures.

A two-step method was applied to locate and quantify vortexes. First, velocity fields were visualized to identify regions of approximately closed circular motion. Potential vortex centers were flagged based on the presence of zero-flow regions surrounded by circular flow patterns (see Figure 4a). Second, the circulation around these centers was calculated by integrating the velocity field along circular paths of varying radii. The maximum circulation was used to confirm the presence of a vortex and to determine its size and strength. Only structures with well-defined closed circulation and a clear maximum in the

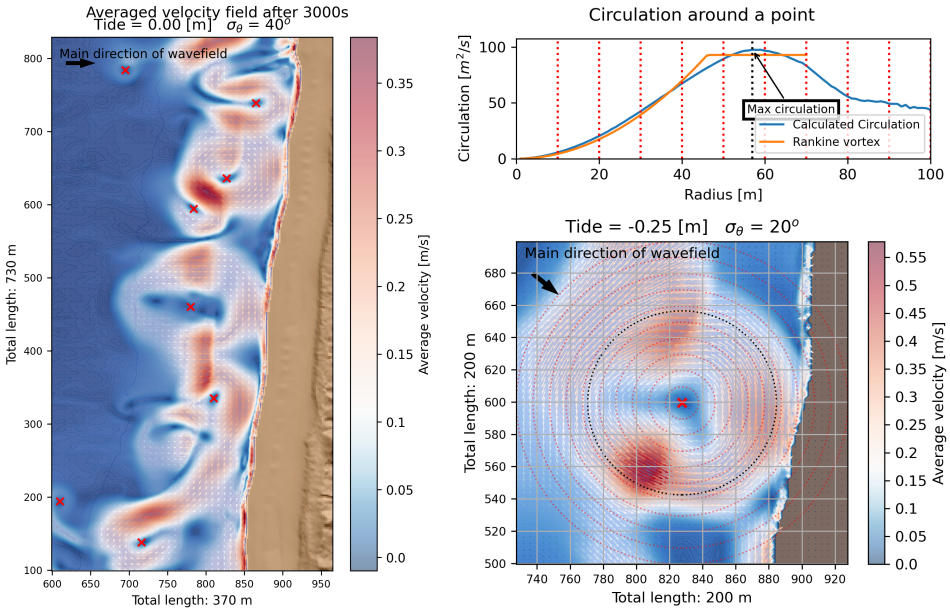

(a) Identifying vortexes **(b) Quantifying a vortex.**

Figure 4: Methodology of identifying and quantifying vortexes. (a) Shows the step of identifying the vortexes. The mean velocities for a section of the domain is plotted alongside markers denoting potential vortexes.(b) Shows the steps of quantifying the vortexes. The bottom figure show the mean velocity field, with the marker showcasing the center of the vortex and thick black circle denoting the radius of maximum circulation. On top the calculated circulation for various radii out from the center is shown along with the best fit Rankine vortex. The radius (R) and strength (Γ_{max}) is marked with an arrow.

circulation-radius relationship were classified as vortexes (See Figure 4b).

Using this methodology, 45 simulations were conducted with varying tidal levels (*tide*), peak wave direction (D_p), and directional spread (σ_θ). Throughout the simulations a total of 343 vortexes were identified.

Rankine vortex

The detected vortexes were compared to idealized Rankine vortexes to characterize their size and strength. A Rankine vortex is a theoretical construct combining solid-body rotation near the center and irrotational flow away from the core. The circulation of a Rankine vortex is defined as:

$$\Gamma(r) = \begin{cases} \Gamma_{\max} r^2/R^2, & \text{if } r \le R, \\ \Gamma_{\max}, & \text{if } r > R, \end{cases}$$

where r is the radial distance from the vortex center, R is the radius of maximum circulation, and Γ_{max} is the maximum circulation. For all the identified vortexes the best fit Rankine vortex was calculated through the method of least squares, resulting in strikingly accurate fits given the non-ideal circumstances of the model vortexes (See Figure 4b for an example).

Approximately 91% of the vortexes identified in the simulations were close to circular, making them well-suited for comparison with Rankine vortexes. For non-circular vortexes, an equivalent radius was computed based on the geometric mean of the semi-major and semi-minor axes. The Rankine vortex framework provided a convenient means of quantifying vortex size (R) and strength (Γ_{max}) enabling direct comparisons across simulations. This systematic approach enabled a robust statistical analysis of vortex characteristics under diverse conditions.

Results

The analysis revealed distinct patterns in vortex size, strength, and count, driven by variations in tidal level, directional spread, and peak wave direction. Statistical analysis with an ANOVA model of 343

detected vortexes confirmed these trends. See Table 1 for a summary of the dependencies.

The tidal level strongly influences the number of vortexes and their sizes. At mid-tide values, the sandbar was optimally submerged, resulting in the largest number of vortexes. Tide levels different from the mean results in fewer vortexes overall. In general, higher tides favor the formation of larger vortexes, while lower tides lead to smaller structures. This trend reflects the role of bathymetry in shaping circulation patterns.

The directional spread (σ_θ) of the incoming wavefield has a pronounced effect on vortex characteristics. It was found that lower directional spreads produce larger and stronger vortexes, as energy was more focused in specific directions. In contrast, higher spreads generated smaller and weaker vortexes due to increased variability in wave breaking and reduced coherence. Interestingly, varying this parameter does not have a significant impact on the number of vortexes observed.

Vortex formation is most pronounced when waves approached the beach perpendicularly $D_p = 0°$. As D_p increases, alongshore currents become dominant, suppressing vortex formation and leading to fewer overall vortexes. Additionally, it was found that while the size of the vortexes remains statistically constant, their strength changes with steeper peak direction.

Response value	Quantity	Size R	Strength Γ_{max}
Increasing parameter			
tide	$\uparrow\downarrow$	$\uparrow$	
σ_θ		$\downarrow$	$\downarrow$
D_p	$\downarrow$		$\downarrow\uparrow$

Table 1: Response diagram of vortex charactheristics.

FLUID PARTICLE PATHS

The study of Bondehagen et al. (2024) was dedicated to showing and discussing the vortex structures and vector fields underlying the vortexes. Here, we are building on the findings and present pathlines of individual fluid particles with the objective to show how they compare them to the oranges' paths and the the vortex structures. We will therefor show and discuss two selected cases, both with the parameters $tide = 0.25$m, $\sigma_\theta = 0$, and $D_P = 20°$.

The first case consists of 800 fluid particles released in a circle of 100m radius around a point identified in the main article as the center of a vortex. This scenario showcases the complex vortex behavior in the surf zone. The second case consists of 100 fluid particles released at the edge of a circle of 10m radius of the same vortex, which illustrates how the pathlines diverge over time.

The particles are released after $T = 600$s, which is long enough for the kinetic and potential energy as well as the enstrophy to reach a stable level. The particles are then transported by the fluid where the Lagrangian velocities are found from a bilinear interpolation of neighboring cells.

Vortex structure

In an effort to explore the interaction between fluid particles and surf zone vortexes, we simulated the release of 800 particles within a 100 m radius around a pre-identified vortex center. This experiment revealed a variety of particle behaviors, demonstrating the complex dynamics of nearshore circulation. The movement of the fluid particles can be seen in Figure 5.

Some particles are immediately transported away from the vortex region, avoiding entrainment altogether. These particles interacted only briefly with the periphery of the vortex, quickly following the surrounding wave-driven currents.

Other particles are temporarily captured by the vortex, completing a single or even multiple revolutions before eventually escaping. These particles initially followed circular trajectories, moving with the coherent structure of the vortex. However, they are eventually carried away by variations in the velocity field, potentially influenced by individual breaking waves, directional spreading, or interactions with bathymetric features. Most of the particles escape downwards along the wave-driven current seen in the mean velocity field, before eventually being transported offshore. This intermediate behavior illustrates the transient nature of vortexes that capture many fluid parcels.

A final group of particles remains within the vortex for a prolonged time. Their extended entrapment

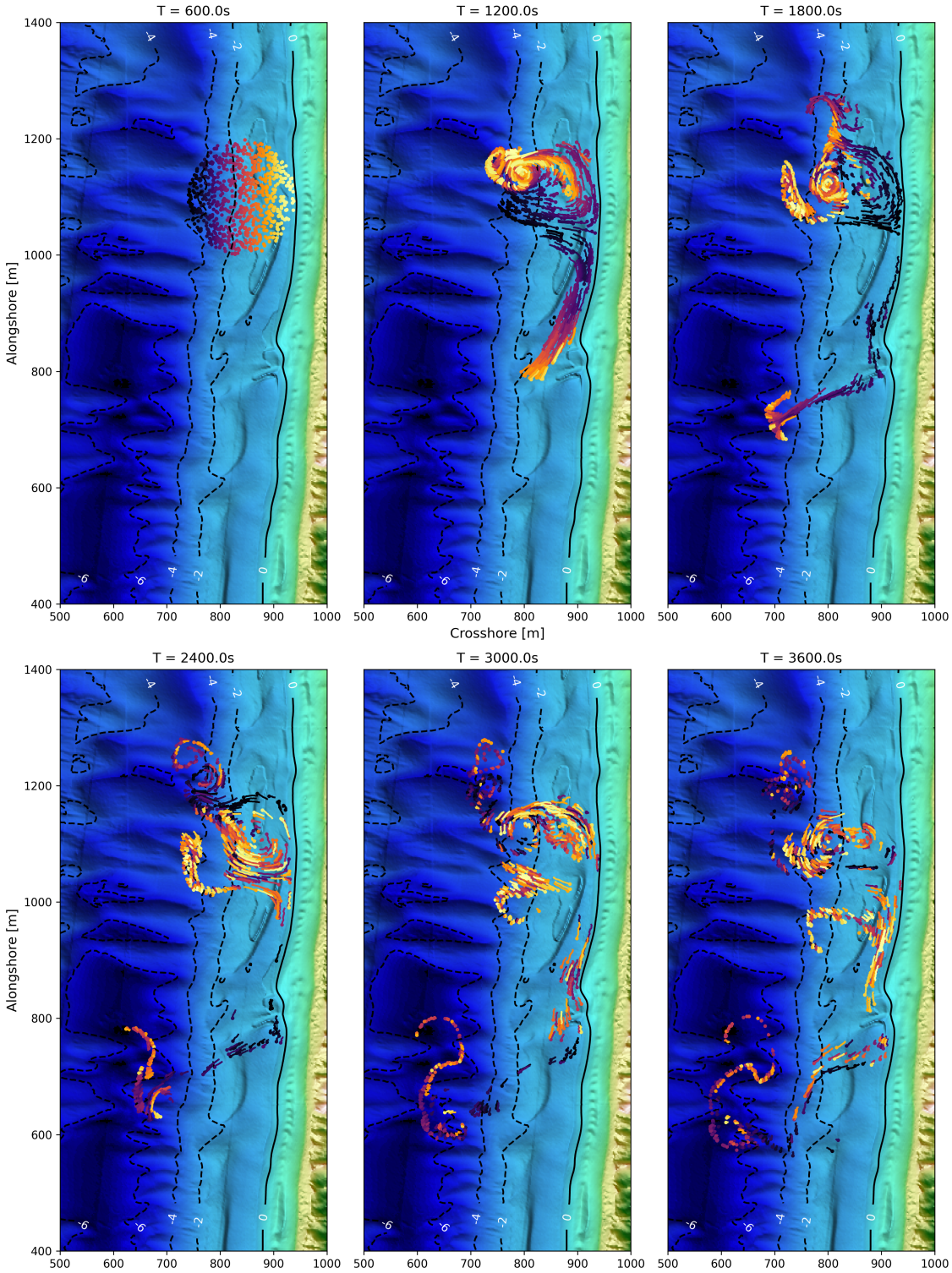

Figure 5: Plot of 800 numerical fluid particles released at $T = 600$s for the specific run of $tide = 0.25$, $\sigma_\theta = 0$, and $D_p = 20°$. The end position of each particle is plotted, together with their location for the previous 60 seconds. In the background the local bathymetry is plotted alongside level curves. The mean velocity for this location can be seen in Figure 6a.

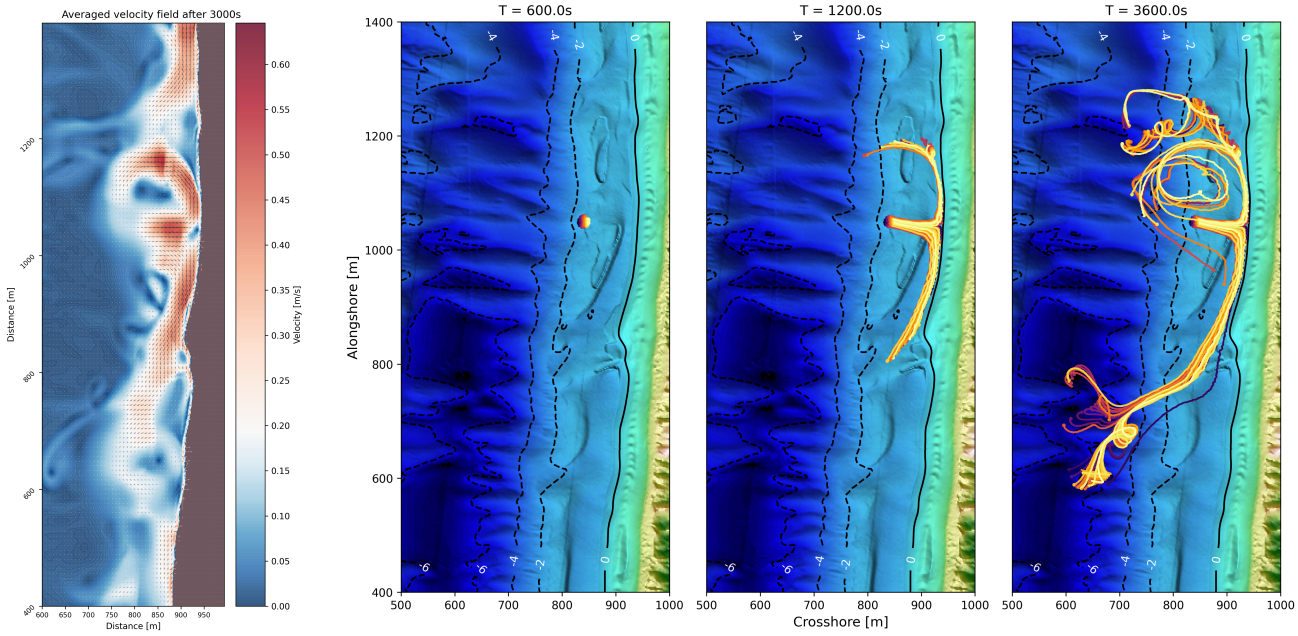

(a) Average velocity field **(b) Pathlines of fluid particles released at $T = 600$s**

Figure 6: Pathlines for 100 numerical fluid particles placed within a circle of 10m radius at the edge of the location of a mean vortex for the same parameters as Figure 5. The mean velocity of this location can be seen in Figure 6a. In figure 6b the pathlines of the numerical particles are plotted alongside bathymetry and bathymetric level curves.

suggests that certain vortexes, under specific environmental conditions, can act as retention zones, keeping fluid and suspended material locally trapped for significant durations.

As shown in the figure, most fluid particles eventually escaped the influence of the vortex. However, as it becomes evident from the mean velocity field in Figure 6a, fluid particles are also transported into the vortex from the outside. Consequently, the vortex structure may represent a temporarily coherent movement of individual particles at any point in time.

The authors believe this supports the validity of the methodology outlined in Bondehagen et al. (2024). While the referenced study focuses on mean velocity fields, the present findings indicate that the vortex structure persists over time spans that cover several wave periods. Although the dynamic structure of the vortex may vary over time, analyzing mean quantities serves as a reliable proxy for understanding the overall behavior of the vortex.

Chaotic motion

A second experiment focuses on the dynamics of particles released in close proximity, with 100 particles deployed within a circle of 10 m radius at the edge of the same vortex (see Figure 6). In contrast to the previous test, this one uses fewer but more densely packed particles. Initially, the particles move together with their trajectories closely aligned. However, over time their paths begin to diverge, with some particles remaining near their initial group while others start moving in markedly different directions. This divergence, however, does not occur gradually or uniformly. Instead, there are extended periods, during which particles remain clustered, followed by abrupt and pronounced dispersal periods.

This pattern of intermittent coherence and sudden separation is indicative of chaotic advection, a phenomenon that has been extensively studied in fluid dynamics and geophysical flows Aref (2002); Ottino (1989). The common element includes an initially ordered configuration of fluid elements that is stretch and fold until it is no longer recognizable, even in 2D laminar flow. In coastal zones, chaotic transport is further influenced by wave dynamics, bathymetry, and transient structures; and therefore it is of no surprise that the flow exhibits some chaotic behavior.

In our simulations, the divergence of particle paths raises intriguing questions. For extended periods,

particles appear to follow coherent trajectories. However, at certain points, small differences in their respective positions or velocities trigger abrupt and significant divergence. The physical mechanisms behind these transitions remain unclear.

These findings highlight the inherent complexity of surf zone dynamics. While the BOSZ model provides a deterministic framework for velocity fields, the particle trajectories reveal characteristics reminiscent of chaotic systems. Such behavior complicates predictions of pollutant dispersion, tracer movement, and material retention in the surf zone, but is nonetheless essential for mixing processes. Future investigations, incorporating both advanced simulations and observational data, are essential to understand why chaotic motion is limited in some regions but amplified in others.

DISCUSSION

The results presented in this paper support and deepen the validation and analysis detailed in Bondehagen et al. (2024), showcasing the BOSZ model's ability to simulate nearshore circulation patterns and expand our understanding of vortex-driven dynamics in the surf zone. The validation efforts, including comparisons with buoy, ADV, and drifter data, demonstrated that a Boussinesq-type model such as BOSZ can reproduce both large-scale and local features of nearshore hydrodynamics. The reconstruction of these measurements provides confidence that the model can be used reliably for studies of wave-induced vortex formation and evolution.

A key outcome of this research is related to the characterization of vortex behavior under varying environmental conditions. The dependencies of vortex size, strength, and occurrence on tidal elevation, wave direction, and directional spread highlight the balance between wave forcing and the influence of bathymetric features. In particular, the tide level modulates the impact of sandbars and other seabed structures, influencing vortex number and size. The directional spread affects the coherence of wave-induced currents, determining whether vortexes emerge as strong and stable features or remain weak and transient. Meanwhile, peak wave direction sets the interplay between longshore currents and vortexes, influencing the number and nature of vortexes present in the surf zone.

The analysis reveals that vortexes can function as short-term retention zones, potentially affecting the distribution of suspended sediments, nutrients, and pollutants. Particles entrained within a vortex may remain trapped for extended periods or escape after multiple revolutions. These findings concur with previous studies (e.g. (Feddersen, 2014; Spydell and Feddersen, 2009; Suanda and Feddersen, 2015; O'Dea et al., 2021)) that have identified vortexes as critical agents for mixing and transport processes in the coastal environment.

Beyond vortex identification, the exploration of fluid particle trajectories provides insight into the complexity of nearshore circulation. While nearby fluid parcels follow similar paths, they sometimes diverge unpredictably, suggesting elements of chaotic advection Aref (2002); Ottino (1989); Brown and Smith (1991). While the previously mentioned articles look at ocean mixing or idealized fluid mechanical problems, the present paper showcases some of the seemingly chaotic features of the wave-induced nearshore flow patterns. The highlighted chaotic behavior complicates the prediction of particle paths, pollutant pathways, and sediment transport, potentially influencing coastal management decisions but also lays out the foundation of surf zone mixing. The results also drive home the challenge in replicating pathlines such as tracked with orange drifters by Bjørnestad et al. (2021). Understanding when and why chaotic dispersion arises remains a challenge. Additional studies utilizing higher-resolution measurements and targeted numerical experiments are necessary to identify the key parameters controlling chaotic dynamics in the surf zone.

CONCLUSION

This papar summarizes the main findings from Bondehagen et al. (2024) which establishes the capabilities od the BOSZ model in reproducing nearshore circulation patterns and vortex dynamics observed at an open beach on Sylt Island. Extending beyond the original work, the new analyses presented here hightlight the complex nature of vortex-particle interactions and the development of chaotic motion. The present work illustrates how the vortex identification methodology captures circular fluid particle trajectories. However, it also exemplifies the difficulties in recreating particle paths for longer periods of time, due to the chaotic behavior inherent in the processes that govern the particles' movement.

These findings have implications for coastal engineering, resource management, and environmental

assessment. Accurately capturing vortex-driven transport, chaotic mixing, and retention zones is essential for predicting sediment pathways, pollutant fate, and the dispersal of biota. The demonstrated capabilities of the BOSZ model lay the groundwork for future studies aimed at isolating and controlling the factors that contribute to vortex formation and chaotic particle behavior, ultimately improving our ability to manage and protect coastal environments.

ACKNOWLEDGEMENTS

We thank Jan Bödewadt and Jurij Stell for technical support. We thank Lutz Christiansen and the LKN.SH (Landesbetrieb für Küstenschutz, Nationalpark und Meeresschutz Schleswig-Holstein) for providing bathymetric data for the bathymetry around Sylt.

We acknowledge funding from the Research Council of Norway under grant no. 239033/F20, from the European Union's Horizon Europe research and innovation programme under the Marie Sklodowska-Curie grant agreement No. 101119437, from Bergen Universitetsfond, from the Coasts in the Changing Earth System (PACES II) program of the Helmholtz Association, and support from the Deutsche Forschungsgemeinschaft (DFG, German Research Foundation, project number 274762653, Collaborative Research centre TRR 181 *Energy Transfers in Atmosphere and Ocean*). Volker Roeber acknowledges financial support from the I-SITE program Energy & Environment Solutions (E2S), the Communauté d'Agglomération Pays Basque (CAPB), and the Communauté Région Nouvelle Aquitaine (CRNA) for the chair position HPC-Waves.

References

H. Aref. The development of chaotic advection. *Physics of Fluids*, 14(4):1315–1325, 2002.

C. M. Baker, M. Moulton, B. Raubenheimer, S. Elgar, and N. Kumar. Modeled three-dimensional currents and eddies on an alongshore-variable barred beach. *Journal of Geophysical Research: Oceans*, 126(7): e2020JC016899, 2021.

M. Bakhoday-Paskyabi. Particle motions beneath irrotational water waves. *Ocean Dynamics*, 65(8):1063–1078, 2015.

M. Bjørnestad, M. Buckley, H. Kalisch, M. Streßer, J. Horstmann, H. Frøysa, O. Ige, M. Cysewski, and R. Carrasco-Alvarez. Lagrangian measurements of orbital velocities in the surf zone. *Geophysical Research Letters*, 48(21):e2021GL095722, 2021.

A. Bondehagen, V. Roeber, H. Kalisch, M. P. Buckley, M. Streßer, M. Cysewski, J. Horstmann, M. Bjørnestad, O. E. Ige, H. G. Frøysa, et al. Wave-driven current and vortex patterns at an open beach: Insights from phase-resolving numerical computations and lagrangian measurements. *Coastal Engineering*, 193: 104591, 2024.

P. Bonneton, D. Lannes, K. Martins, and H. Michallet. A nonlinear weakly dispersive method for recovering the elevation of irrotational surface waves from pressure measurements. *Coastal Engineering*, 138:1–8, 2018.

H. Borluk and H. Kalisch. Particle dynamics in the KdV approximation. *Wave Motion*, 49(8):691–709, 2012.

J. A. Brown, J. H. MacMahan, A. J. Reniers, and E. B. Thornton. Field observations of surf zone–inner shelf exchange on a rip-channeled beach. *Journal of Physical Oceanography*, 45(9):2339–2355, 2015.

M. G. Brown and K. B. Smith. Ocean stirring and chaotic low-order dynamics. *Physics of Fluids A: Fluid Dynamics*, 3(5):1186–1192, 1991.

B. Castelle, T. Scott, R. Brander, and R. McCarroll. Rip current types, circulation and hazard. *Earth-Science Reviews*, 163:1–21, 2016.

Q. Chen, J. T. Kirby, R. A. Dalrymple, F. Shi, and E. B. Thornton. Boussinesq modeling of longshore currents. *Journal of Geophysical Research: Oceans*, 108(C11), 2003.

J. Choi, J. T. Kirby, and S. B. Yoon. Boussinesq modeling of longshore currents in the sandyduck experiment under directional random wave conditions. *Coastal Engineering*, 101:17–34, 2015.

D. B. Clark, F. Feddersen, and R. Guza. Modeling surf zone tracer plumes: 2. transport and dispersion. *Journal of Geophysical Research: Oceans*, 116(C11), 2011.

C. G. David, A. Hennig, B. M. Ratter, V. Roeber, T. Schlurmann, et al. Considering socio-political framings when analyzing coastal climate change effects can prevent maldevelopment on small islands. *Nature Communications*, 12(1):1–19, 2021.

R. Davidson-Arnott, B. Bauer, and C. Houser. *Introduction to coastal processes and geomorphology*. Cambridge university press, 2019.

F. Feddersen. The generation of surfzone eddies in a strong alongshore current. *Journal of Physical Oceanography*, 44(2):600–617, 2014.

F. Feddersen, D. B. Clark, and R. Guza. Modeling surf zone tracer plumes: 1. waves, mean currents, and low-frequency eddies. *Journal of Geophysical Research: Oceans*, 116(C11), 2011.

J.-F. Filipot, P. Guimaraes, F. Leckler, J. Hortsmann, R. Carrasco, E. Leroy, N. Fady, M. Accensi, M. Prevosto, R. Duarte, et al. La Jument lighthouse: a real-scale laboratory for the study of giant waves and their loading on marine structures. *Philosophical Transactions of the Royal Society A*, 377(2155):20190008, 2019.

K. Hally-Rosendahl and F. Feddersen. Modeling surfzone to inner-shelf tracer exchange. *Journal of Geophysical Research: Oceans*, 121(6):4007–4025, 2016.

K. Hally-Rosendahl, F. Feddersen, D. B. Clark, and R. Guza. Surfzone to inner-shelf exchange estimated from dye tracer balances. *Journal of Geophysical Research: Oceans*, 120(9):6289–6308, 2015.

D. L. Inman and B. M. Brush. The coastal challenge. *Science*, 181(4094):20–32, 1973.

H. Kalisch, F. Lagona, and V. Roeber. Sudden wave flooding on steep rock shores: a clear but hidden danger. *Natural Hazards*, pages 1–21, 2024.

B. E. Larsen, M. A. A. Al-Obaidi, H. G. Guler, S. Carstensen, K. D. Goral, E. D. Christensen, N. B. Kerpen, T. Schlurmann, and D. R. Fuhrman. Experimental investigation on the nearshore transport of buoyant microplastic particles. *Marine Pollution Bulletin*, 187:114610, 2023.

N. Li, V. Roeber, Y. Yamazaki, T. W. Heitmann, Y. Bai, and K. F. Cheung. Integration of coastal inundation modeling from storm tides to individual waves. *Ocean Modelling*, 83:26–42, 2014.

P. J. Lynett, K. Gately, R. Wilson, L. Montoya, D. Arcas, B. Aytore, Y. Bai, J. D. Bricker, M. J. Castro, K. F. Cheung, et al. Inter-model analysis of tsunami-induced coastal currents. *Ocean Modelling*, 114:14–32, 2017.

D. Morichon, V. Roeber, M. Martin-Medina, F. Bellafont, and S. Abadie. Tsunami Impact on a Detached Breakwater: Insights from Two Numerical Models. *Journal of Waterway, Port, Coastal, and Ocean Engineering*, 147(2):05021001, 2021.

J.-R. Nader, A. Fleming, G. Macfarlane, I. Penesis, and R. Manasseh. Novel experimental modelling of the hydrodynamic interactions of arrays of wave energy converters. *International Journal of marine energy*, 20:109–124, 2017.

A. O'Dea, N. Kumar, and M. C. Haller. Simulations of the surf zone eddy field and cross-shore exchange on a nonidealized bathymetry. *Journal of Geophysical Research: Oceans*, 126(5):e2020JC016619, 2021.

J. M. Ottino. *The kinematics of mixing: stretching, chaos, and transport*, volume 3. Cambridge University Press, 1989.

J. Pinault, D. Morichon, and V. Roeber. Estimation of Irregular Wave Runup on Intermediate and Reflective Beaches Using a Phase-Resolving Numerical Model. *Journal of Marine Science and Engineering*, 8(12): 993, 2020.

U. Putrevu and I. A. Svendsen. Three-dimensional dispersion of momentum in wave-induced nearshore currents. *European Journal of Mechanics-B/Fluids*, 18(3):409–427, 1999.

G. Rilov, S. E. Dudas, B. A. Menge, B. A. Grantham, J. Lubchenco, and D. R. Schiel. The surf zone: a semi-permeable barrier to onshore recruitment of invertebrate larvae? *Journal of Experimental Marine Biology and Ecology*, 361(2):59–74, 2008.

J. D. Roberts, C. Jones, and J. Magalen. Wave energy converter (wec) array effects on wave current and sediment circulation: Monterey bay ca. Technical report, Sandia National Lab.(SNL-NM), Albuquerque, NM (United States), 2014.

V. Roeber and J. D. Bricker. Destructive tsunami-like wave generated by surf beat over a coral reef during Typhoon Haiyan. *Nature Communications*, 6, 08 2015.

V. Roeber and K. F. Cheung. Boussinesq-type model for energetic breaking waves in fringing reef environments. *Coastal Engineering*, 70:1–20, 2012a.

V. Roeber and K. F. Cheung. BOSZ (Boussinesq Ocean and Surf Zone model). *NOAA Special Report, Proceedings and Results of the 2011 NTHMP Model Benchmarking Workshop*, pages 1–437, 2012b.

V. Roeber, K. F. Cheung, and M. H. Kobayashi. Shock-capturing boussinesq-type model for nearshore wave processes. *Coastal Engineering*, 57(4):407–423, 2010.

T. Scott, G. Masselink, M. J. Austin, and P. Russell. Controls on macrotidal rip current circulation and hazard. *Geomorphology*, 214:198–215, 2014.

A. L. Shanks, S. G. Morgan, J. MacMahan, and A. J. Reniers. Surf zone physical and morphological regime as determinants of temporal and spatial variation in larval recruitment. *Journal of Experimental Marine Biology and Ecology*, 392(1-2):140–150, 2010.

M. Spydell and F. Feddersen. Lagrangian drifter dispersion in the surf zone: Directionally spread, normally incident waves. *Journal of Physical Oceanography*, 39(4):809–830, 2009.

M. Spydell, F. Feddersen, R. Guza, and W. Schmidt. Observing surf-zone dispersion with drifters. *Journal of Physical Oceanography*, 37(12):2920–2939, 2007.

M. S. Spydell, F. Feddersen, and R. Guza. Observations of drifter dispersion in the surfzone: The effect of sheared alongshore currents. *Journal of Geophysical Research: Oceans*, 114(C7), 2009.

S. H. Suanda and F. Feddersen. A self-similar scaling for cross-shelf exchange driven by transient rip currents. *Geophysical Research Letters*, 42(13):5427–5434, 2015.

I. A. Svendsen. *Introduction to nearshore hydrodynamics*, volume 24. World Scientific, 2006.

A. Varing, J.-F. Filipot, M. Delpey, G. Guitton, F. Collard, P. Platzer, V. Roeber, and D. Morichon. Spatial distribution of wave energy over complex coastal bathymetries: development of methodologies for comparing modeled wave fields with satellite observations. *Coastal Engineering*, page 103793, 2020.

A. Varing, J.-F. Filipot, S. Grilli, R. Duarte, V. Roeber, and M. Yates. A new definition of the kinematic breaking onset criterion validated with solitary and quasi-regular waves in shallow water. *Coastal Engineering*, 164:103755, 2021.

M. Watanabe, K. Goto, V. Roeber, and F. Imamura. Identification of coastal sand deposits from tsunamis and storm waves based on numerical computations. *Journal of Geophysical Research: Earth Surface*, 126(7):1–20, 2021.

W.-Y. Wong, M. Bjørnestad, C. Lin, M.-J. Kao, H. Kalisch, P. Guyenne, V. Roeber, and J.-M. Yuan. Internal flow properties in a capillary bore. *Phys. Fluids*, 31(11), 2019.